Supplementary Data

1. The constitutive model for a neo-Hookean solid (Ogden, 1978)

Consider the multiplicative decomposition of deformation gradient $\mathbf{F}$ into a volumetric part $J^{1/3}\mathbf{I}$ and an isochoric part $\mathbf{F}^u = J^{-1/3}\mathbf{F}$, where $J = \det(\mathbf{F})$ and $\mathbf{I}$ the unit matrix. The Cauchy-Green stress, $\boldsymbol{\sigma}_p$, can be calculated as

$$\sigma_{pij} = \bar{\kappa}(J-1)\delta_{ij} + \frac{\bar{E}}{3J}\left(B_{ij} - \frac{1}{3}trace(B_{ij})\delta_{ij}\right) \tag{S1}$$

where δ_{ij} is the Kronecker delta, $\bar{E}$ the initial elastic modulus , $\bar{\kappa}$ the bulk modulus and $\mathbf{B}$ the deviatoric left Cauchy-Green deformation tensor, $\mathbf{B} = \mathbf{F}^u \bullet \mathbf{F}^{uT}$.

2. The model for focal adhesion

A simplified model is employed to simulate focal adhesion between a cell and the underlying extracellular matrix (ECM). Let k_o represent the effective spring constant of a single ligand-receptor bond and ψ the concentration of ligand-receptor bonds per unit cell membrane area. The traction, $\mathbf{T}$, on surface areas associated with the contact points on the cell membrane and ECM reads

$$\mathbf{T} = k_o \psi \delta_o \boldsymbol{\alpha} \tag{S2}$$

where k_o is the effective stiffness of a single ligand-receptor bond, $k_o \sim 1\,\text{nN}\,\mu\text{m}^{-1}$ (Dembo, 1994), δ_o is the relative displacement of the contact points and $\boldsymbol{\alpha}$ the unit vector representing the direction of $\mathbf{T}$, as schematically shown in Figure S1. The value of ψ is governed by the thermo-dynamical process as described by Pathak et al. (2008). To make it simple, ψ is assumed to be a constant value, i.e. $\psi = 3333\,\mu\text{m}^{-2}$, which is estimated based on the numerical studies reported by McGarry et al.(2009) and Pathak et al. (2008).

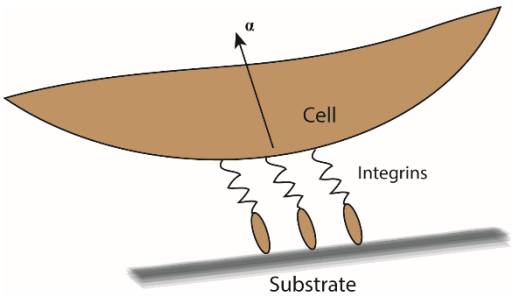

Figure S1 Schematics of cell-substrate interaction via focal adhesion complexes

For vMTFs with micropatterned tissues as discussed in Section 3, numerical studies with three selected values of k_o, namely, $k_o = 0.015, 0.15, 1.5\,\text{nN}\,\mu\text{m}^{-1}$, has been conducted in order to understand its effect. For brevity, the simulation results are not shown here. These simulation results demonstrate the response of vMTFs is not sensitive to k_o. For endothelial cells resting on an array of micro-posts, Figure S2 shows the time history of strain energy under stimulation of LPA ($10\,\mu\text{g mL}^{-1}$) and three selected values of k_o, i.e. $k_o = 0.015, 0.15, 1.5\,\text{nN}\,\mu\text{m}^{-1}$. Strain energy is again not sensitive to the value of k_o when $k_o \sim 1\,\text{nN}\,\mu\text{m}^{-1}$. However, the effect of k_o becomes significant when $k_o \sim 0.1\text{-}0.01\,\text{nN}\,\mu\text{m}^{-1}$.

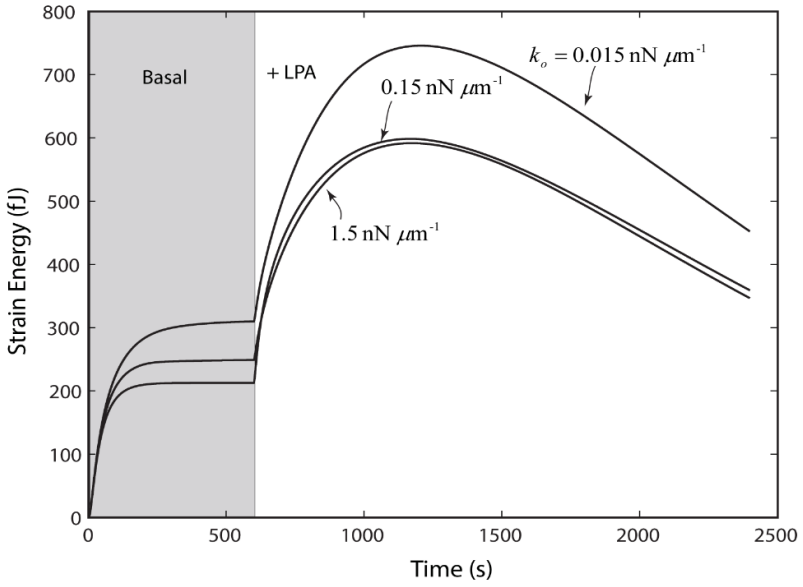

Figure S2 Time history of strain energy of an endothelial cell resting on an array of micro-posts subjected to stimulation of LPA ($10\ \mu\text{g mL}^{-1}$), obtained by simulation with selected values of k_o.

3. Numerical simulation on novel designs of micropatterned vMTFs

Motivated by Murphy (1988), the designs of the vMTFs with micropatterned tissues in three types of arrangements are proposed in Fig. S3(*a*). These designs represent combination of series and parallel linkages of cells in a tissue either in symmetrical arrangement, i.e. Arrangement II and III, or in staggered arrangement, i.e. Arrangement I. Figure S3 (b) shows the time histories of radius of curvature of these vMTFs, measured at the centre of the vMTFs with b = 100 μm and d = 100 μm, when subjected to the time histories of agonist and inhibitor described in Figure 4 (a). Even though the maximum principle stresses within these tissues are all identical owing to isometric deformation, the deformations output of these vMTFs are different: symmetrical arrangement, such as Arrangement II and III, generates greater change of curvatures than the staggered arrangement in Arrangement I. The vMTFs with staggered tissue arrangement have bend-twist coupled deformation mode while vMTFs with symmetrical tissue arrangement have bending dominated deformation mode. Figure S3(*c*) shows the evolution of the orientation of $\eta_{\max}$ within the selected tissues of the three types of vMTFs, which is found to be nearly identical to the orientation of the maximum principal stress. For the micropatterned tissues with large aspect ratio, i.e. the ratio of length to width, the orientation of $\eta_{\max}$ evolves from the longitudinal direction to the transverse direction of the microtissues as time increases, see Arrangement I and II. However, for smaller aspect ratio such as Arrangement III, the mutual influence of the micropatterned tissues becomes significant and the orientation of $\eta_{\max}$ no longer evolves from the longitudinal direction to the transverse direction.

(a)

(I)

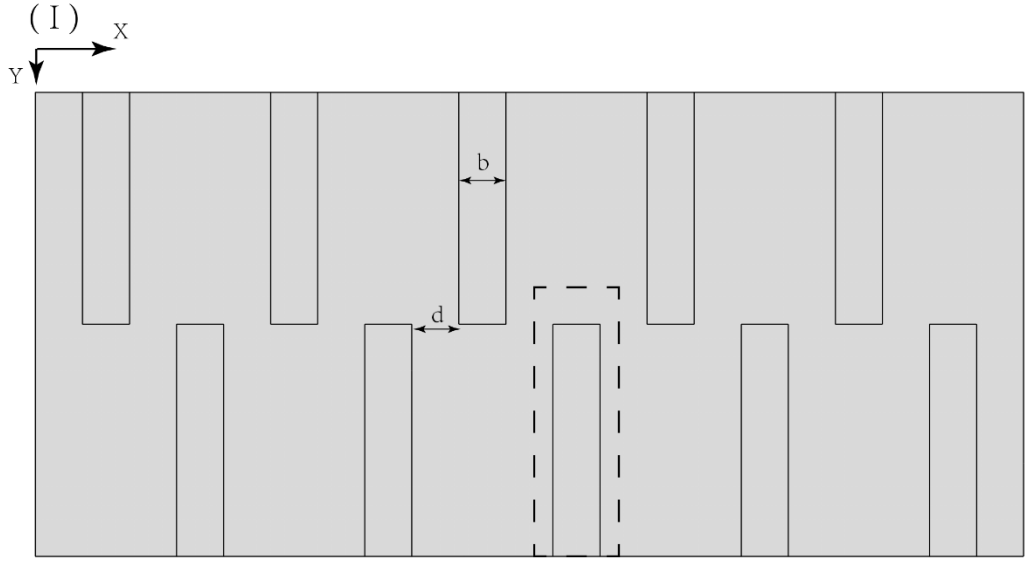

(II)

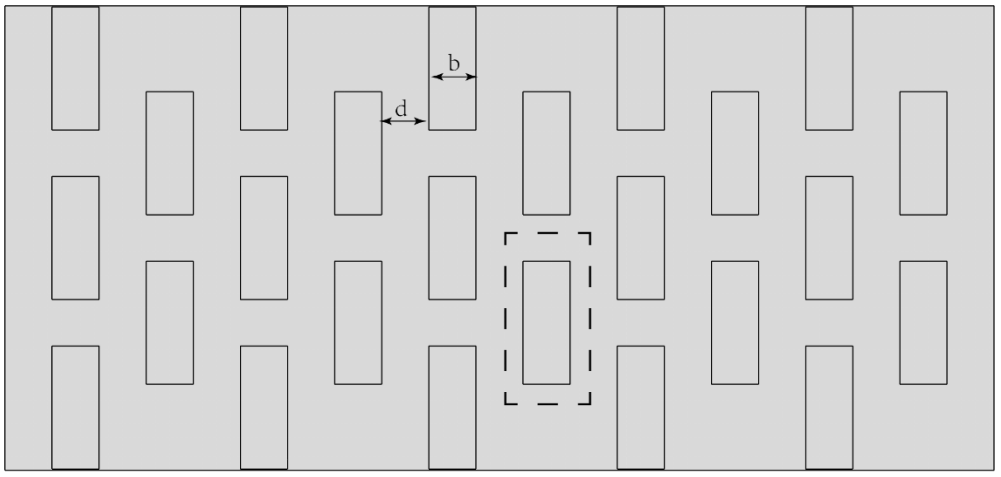

(III)

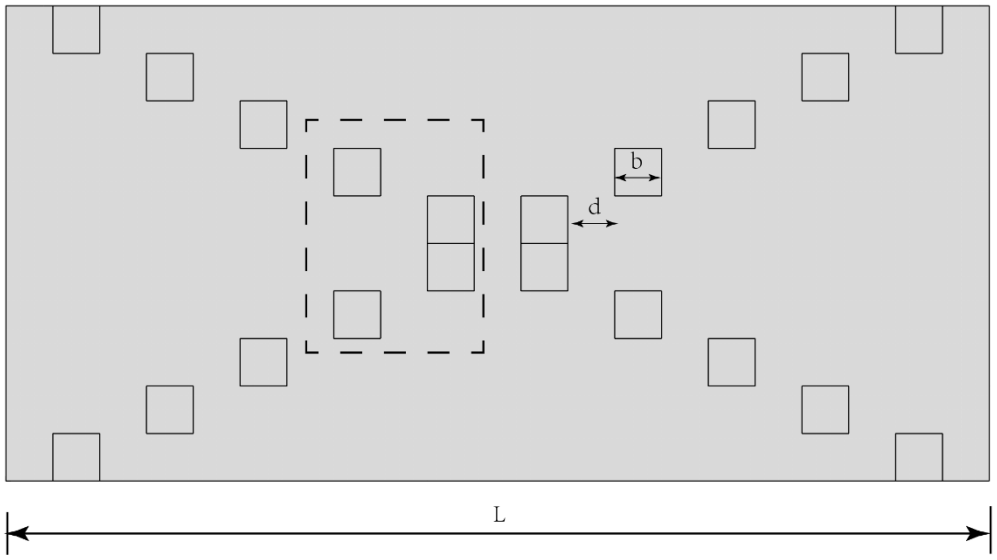

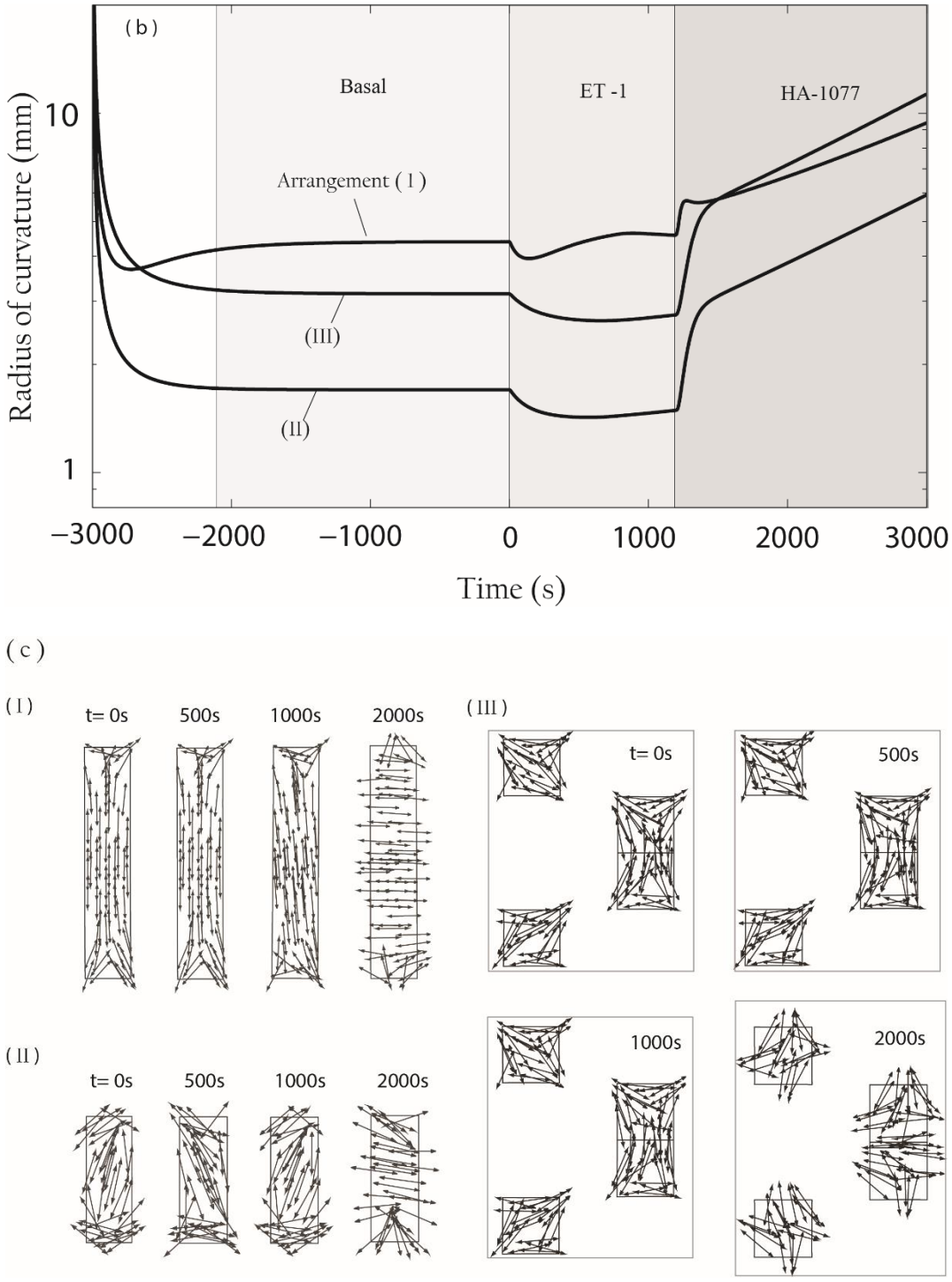

Figure S3 (a) vMTFs with micropatterned tissues in three types of arrangements, (b) time histories of radius of curvature of the vMTFs, measured at the centre of the vMTFs, when subjected to the time histories of agonist and inhibitor described in Figure 4 (a), and (c) the orientation of $\eta_{\max}$ within the microtissues in the three types of vMTFs at selected time instants. The location of the microtissues has been highlighted in (a) using dashed lines.

4. Parameter study on the effects of rate constants to response of vMTFs

In the simulations reported in Section 3, Ca^{2+}/MLCK pathway was considered through rate constants k_1 and k_6. Figure 4 (a) shows the calibrated time histories of k_1 and k_6 employed in the simulation, which can be described in the Eq.(14). However, as reviewed by Katoh, et al. (2011), contraction of stress fibres can also be regulated by Ca^{2+}- independent Rho kinase pathway. In the SMCs based model described in Eqs. (1) through (4), Ca^{2+}- independent Rho kinase pathway can be modelled through rate constants k_2, k_5, k_3 and k_4 (Liu, 2014). In the simulation reported in Section 3, these constants were estimated based on Hai and Murphy (1988), i.e. $k_2 = k_5 = 0.5\,\mathrm{s}^{-1}$, $k_3 = 0.4\,\mathrm{s}^{-1}$, $k_4 = 0.1\ \mathrm{s}^{-1}$. To understand the effects of these key rate constants, parameter study has been conducted via the numerical simulations of monolayered vMTFs. The finite element model is described in Section 3 and the results are shown in Fig.S4. In the parameter study simulations, three values of a selected rate constant were employed without altering other rate constants. It is demonstrated that the numerical results are sensitive to these rate constants. Further research will focus on modelling on Ca^{2+}- independent Rho kinase pathway via rate constants k_2, k_5, k_3 and k_4.

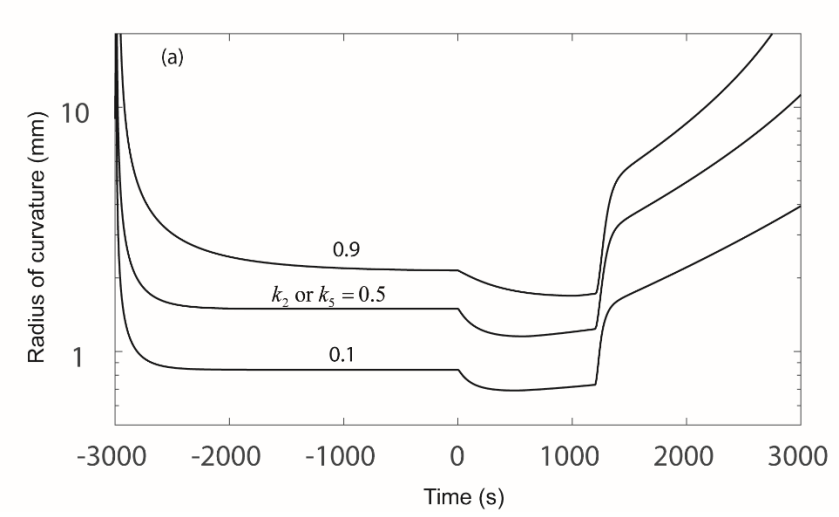

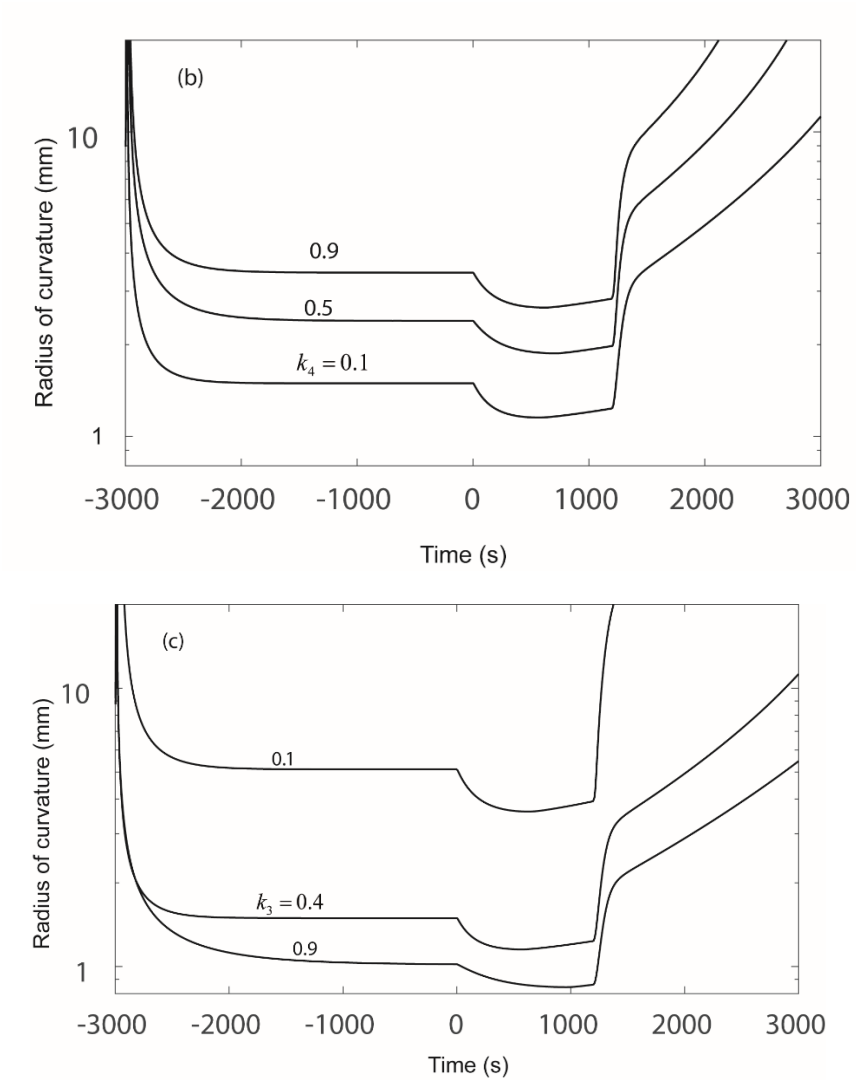

Figure S4 Response of vMTFs with a monolayered tissue under stimulation of ET-1 for 1200 s followed by HA1022. (a) $k_2 = k_5 = 0.1, 0.5, 0.9$; (b) $k_4 = 0.1, 0.5, 0.9$; and (c) $k_3 = 0.1, 0.4, 0.9$.

5. Simulation of endothelial cells on an array of micro-posts under stimulation of VEGF

The experimental results indicated some agonists, such as Histamine and VEGF, could cause significant increases in actin polymerization, even though they had little effect on the level of phosphorylation of myosin light chain II (Yang, et al., 2011). Increase of actin polymerization essentially increases the number of myosin-binding sites on actin filaments and, therefore, increases the attachment rate of myosin to actin filaments. Hence, the effects of Histamine and VEGF can be reflected through the time history of k_3. As the experimental study reported by Yang, et al. (2011), the responses of the endothelial cells under the effect of VEGF are scattered: approximately 30 percent of the cells experienced only a gradual smooth increase in strain energy while 50 percent cells rapidly spiked after VEGF stimulation. In this paper, the following function is employed to simulate time history of k_3 for stimulation of 50 ng mL^{-1} VEGF, which is used to simulate the smooth response of the cells.

$$k_3 = \begin{cases} 0.2 & t < 600\,\mathrm{s} \\ 0.85\left[1-\exp\left(-\dfrac{t-425}{620}\right)\right]\left[0.99\exp\left(-\dfrac{t}{16000}\right)+0.01\right] & 600\,\mathrm{s} \le t \le 2400\,\mathrm{s} \end{cases} \tag{S3}$$

In Eq. (S3), the initial value of k_3 ($t < 600\,\mathrm{s}$) is defined for basal response and the value for $600\,s \le t \le 2400\,\mathrm{s}$ is defined for the effect of VEGF. The time history of k_1 keeps at the basal level, namely, k_1 = 0.045 s^{-1}. The simulation results are shown in Figs. S5 (a) and (b) for the time history of strain energy stored in the endothelial cell and the corresponding contours of strain energy density at selected time instants, respectively, in comparison with experimental measurement. Even though the geometry of the substrate was not modelled with details, the agreement between the simulation and the experiment is reasonably good. Similar to the response under stimulation of k_1, the deformation of the cell diminishes from the edge to the centre and the central part of the cell is under isometric state.

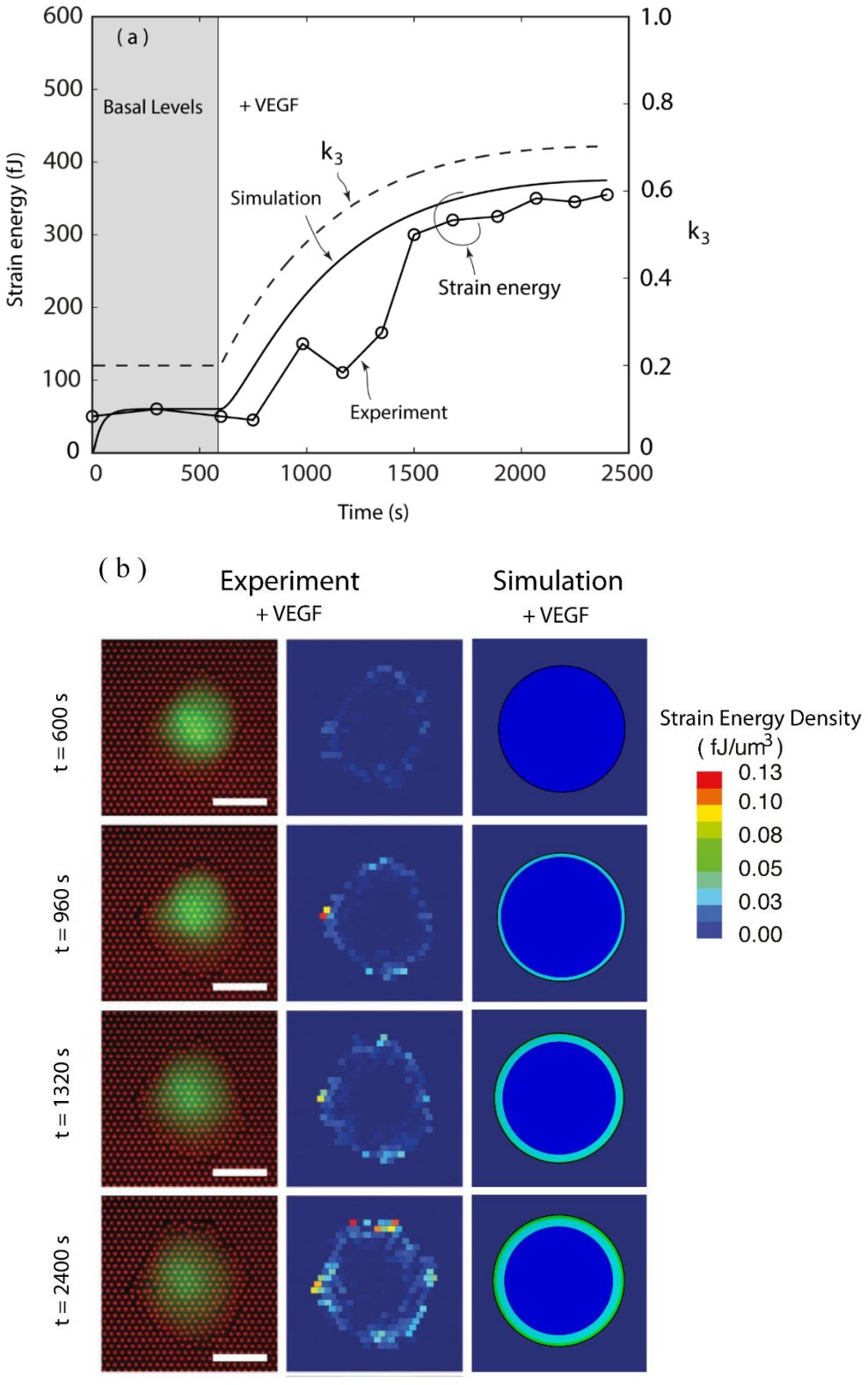

Figure S5 Mechanical response of an endothelial cell resting on an array of micro-posts subjected to stimulation of VEGF (50 ng mL^{-1}). (a)Time histories of k_3 employed in the numerical calculation and strain energy stored in the cell obtained by experiment (Yang et al.2011, reproduced by permission of The Royal Society of Chemistry) and the numerical simulation, respectively; (b) contours of strain energy density of the cell obtained by the experiment nd numerical simulation, respectively, at

selected time instants . Scale bars are 30 μm . For interpretation of the color legend in this figure, the reader is referred to the web version of this article.

References

Dembo M. 1994 On peeling an adherent cell from a surface. In Vol. 24 of series: Lectures on mathematical problem in Biology, American Mathematical Society, Providence, RI, 51-77.

Katoh, K., Kano, Y. and Noda, Y., 2011. Rho-associated kinase-dependent contraction of stress fibres and the organization of focal adhesions. Journal of The Royal Society Interface, **8**(56), pp.305-311.

Murphy RA. 1988 Muscle cells of hollow organs. News Physiol. Sci. **3**, 124–128.

Ogden RW. 1978 Nearly isochoric elastic deformations: application to rubberlike solids. J. Mech. Phys. Solids, **26**, 37–57.

Yang MT, Reich DH, Chen CS. 2011 Measurement and analysis of traction force dynamics in response to vasoactive agonists. Integr. Biol. **3**, 663–674.

Liu T. 2014 A constitutive model for cytoskeletal contractility of smooth muscle cells. Proceedings of the Royal Society of London A. **470**, 2164